

A New Method for 3D Modeling of Joint Surface Degradation and Void Space Evolution Under Normal and Shear Loads

Yang Gui¹ · Caichu Xia^{1,2} · Wenqi Ding¹ · Xin Qian¹ · Shigui Du²

Received: 27 March 2017 / Accepted: 20 May 2017 / Published online: 30 May 2017
© Springer-Verlag Wien 2017

Keywords Joint surface · Void space · Degradation · Evolution

1 Introduction

The roughness of the joint surfaces strongly influences the mechanical and hydraulic behavior of the joints, especially under shearing. Once shearing is initiated, only certain fractions of the joint surfaces remain in contact and every asperity contributes to the shear behavior depending on their respective heights and dip angles. In addition, several asperities would be damaged, and the debris accumulate and form gouge in the joint surface upon shearing (Ladanyi and Archambault 1970; Archambault et al. 1997; Riss et al. 1997; Belem et al. 2007), so the joint surface topography, and the void space which is comprised of the separation and the contact between two rough surfaces, continuously change with shearing. In the majority of the analyses of the joint shearing behavior, joint roughness has been characterized based on the initial joint surfaces and remained constant regardless of shearing (Grasselli and Egger 2003; Belem et al. 2009; Asadollahi and Tonon 2010; Zandarin et al. 2013; Park et al. 2013). In most analyses of the coupled shear-flow properties of joints during shearing, the mean aperture (the mean separation between two rough joint surfaces) was characterized by adding a changing normal

displacement to an initial aperture (Bandis et al. 1983; Olsson and Barton 2001; Koyama et al. 2006; Li et al. 2008). This treatment ignores the asperity damage, debris accumulation, and the dislocation of the two surfaces. Thus, roughness parameters and void space characterization should be redefined based on the damage of joint surfaces during shearing.

Goodman (1989) reviews the joint surface roughness measurement methods which are useful to engineers, but these methods can only be used to joint surface measurement without shearing. Experimental methods have been proposed to measure the void space or contact areas of rock joints (Gentier et al. 1989; Yeo et al. 1998; Kulatilake et al. 2006, 2008). These methods involve inserting or injecting different materials (Gentier et al. 1989; Nemoto et al. 2009; Park and Song 2013) between the joint surfaces, but these methods can only be used in joint compression tests without shearing. Numerical method has also been employed to calculate joint aperture and contact area (Koyama et al. 2006; Park and Song 2013; Xia et al. 2014a; Fathi et al. 2015). This method initially acquires the joint surface data before fixing the lower surface and moves the upper surface according to the normal and shear displacements in the joint shear test; the overlapping areas of the two displaced surfaces are deleted because these areas are considered as damaged. This treatment ignores the elastic and/or plastic deformation of the asperity. Hans and Boulon (2003) reported a new device that can measure the joint surface during shearing by stopping the test and separating the two surfaces. However, the method destroys the stress state of the joint, which influences the subsequent shear mechanical behavior of the joint. Indraratna et al. (2014) obtained the joint surface asperity deformation by measuring the joint surface before and after a shear test, while the surface data and joint aperture distribution during shearing could not be acquired by this method.

✉ Caichu Xia
tjxiaccb@126.com

¹ Department of Geotechnical Engineering, Tongji University, Shanghai 200092, People's Republic of China

² College of Civil Engineering, Shaoxing University, Shaoxing 312000, Zhejiang, People's Republic of China

We introduce in the present paper a new method to capture the joint surface deformation and aperture distribution during shearing. The specimen preparation is presented in Sect. 2. Section 3 introduces the joint surface measurement and direct shear test procedure. The detail of the new method to compute the joint surface deformation and aperture distribution during shearing is presented in Sect. 4. In Sect. 5, verification of the method and test results is presented and briefly discussed. Conclusions are drawn in Sect. 6.

2 Specimen Preparation

Identical replicas of a natural granite joint surface were used to control the independent factors affecting the joint shear behavior. The natural joint used here was unweathered matching tensile joint collected from a tunnel engineering. The natural granite joint was cut into a planar dimension of $200 \times 100 \text{ mm}^2$ and placed into a steel box with an internal dimension of $200 \times 100 \times 100 \text{ mm}^3$. We first duplicated the rock joint surface with silicone rubber to accurately reproduce the parent joint surface with sufficient strength and longevity. The rubber mold was turned over and again placed into the steel box after 24 h. The mated rubber molds were prepared by pouring silicone rubber into the steel box. The two surfaces of a specimen were made by copying the two rubber molds with plaster mixture (a mixture of plaster, water, and additive with a weight ratio of 3:1:0.01). Thus, mated plaster joint samples with a dimension of $200 \times 100 \times 100 \text{ mm}^3$ were prepared. The mechanical properties of the plaster material were estimated by conducting uniaxial compression and Brazilian tests on the 70.7 mm cubic specimens and the 50 mm diameter circular disk specimens (thickness/diameter = 0.5), respectively. The basic friction angle was measured through tilt table tests on the dry saw-cut surface of three specimens. Test results can be found in Table 1. The joint surfaces were dyed red so that the damaged area could be easily distinguished from the undamaged area. A total of six specimens were prepared and cured at a constant temperature of 25 °C for 7 days.

3 Testing Procedure

3.1 Joint Surface Measurement

This study used an advanced 3D fringe projection optical measuring system, the TJXW-3D portable rock surface

topography scanner, to acquire 3D coordinates of the joint surfaces. The system comprises a measuring head, a tripod, a computer, and a standard calibration plate. The measuring head, including a fringe projector and two CCD cameras, is screwed on the top of the tripod and placed approximately 50 cm above the object with the head down (Fig. 1a). Details of the measurement system can be found in Xia et al. (2014b). The accuracy of single scanning of this system is less than 0.02 mm. Figure 1c shows an example of a digital joint surface.

3.2 Direct Shear Test

In our study, all specimens were replicated from one mated rubber joint mold and thus had identical surface topography. Moreover, results of tests conducted under the same load condition, including the damage degree and distribution of asperity deformation, with specimens made from one material should also be ideally identical. Thus, we conducted several direct shear tests that were stopped at different shear displacements to capture the joint surface topography during shearing without destroying the stress state of the joint. The joint surface topography during shearing could be represented by the specimens that were stopped at the corresponding shear displacement. A direct shear test was first performed until reaching the residual shear strength state to determine the shear displacements of the key stress state. The following shear tests were stopped at the predefined shear displacements each of a new specimen.

The applied normal stress was 1 MPa, which corresponds to the realistic normal stress found in practice, and the shear displacement rate was kept at 0.5 mm/min throughout each test.

4 Computation of Joint Surface Degradation and Void Space

The TJXW-3D scanner was used to digitize the specimen in the closed position and two halves individually. In acquiring each of these digital surfaces, multiple measurements were taken from different directions because only points simultaneously visible in two cameras could be recorded in a single measurement. With permanent reference points attached to the sides of the joint samples, the software automatically transferred the subsequent measurements into the coordinate system of the first measurement.

Table 1 Basic mechanical properties of plaster material

Tensile strength/MPa	Compressive strength/MPa	Young's modulus/GPa	Basic friction angle/°
1.26 ± 0.10	24.53 ± 2.07	6.00 ± 0.54	38.03 ± 2.94

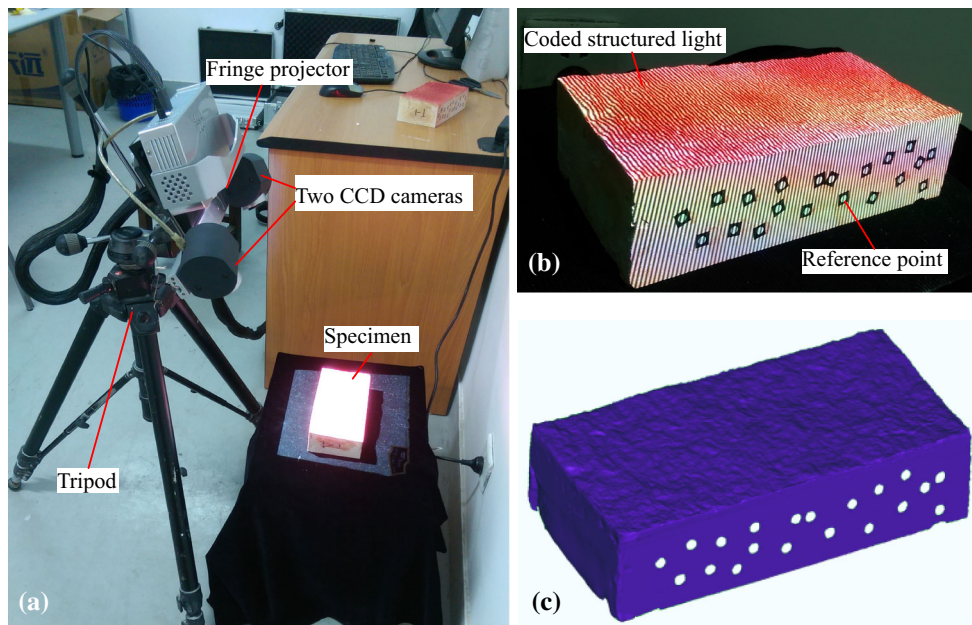


Fig. 1 **a** TJXW-3D portable rock surface topography scanner, **b** specimen surface with coded structured light projected by fringe projector, **c** example of a digital joint surface

1. The alignment of the joint surface data before and after the shear tests was established by transferring the coordinate of the joint surface data after the test to that of the initial joint surface data before the test (Fig. 2a). Consequently, the surface height deviation ($z_{\text{deviation}}$) between the initial joint surface and the joint surface after shear test was calculated as

$$z_{\text{deviation}}(x_i, y_i) = z_{\text{initial}}(x_i, y_i) - z_{\text{after}}(x_i, y_i) \quad (1)$$

where $z_{\text{initial}}(x_i, y_i)$ is the surface height of the initial joint surface, $z_{\text{after}}(x_i, y_i)$ is the surface height of the joint surface after the shear test, and x_i and y_i are the plane coordinates. If the asperity was severely damaged and the debris from the broken asperity was crushed and moved away, then the calculated $z_{\text{deviation}}$ would be considerably positive. Moreover, if the crushed material from the broken asperity had been accumulated and compacted on the surface, then the $z_{\text{deviation}}$ value would be significantly negative. Theoretically, $z_{\text{deviation}} = 0$ indicates that the asperity was neither damaged nor had accumulated debris. While as stated in the beginning of this section, multiple measurements were required from different directions to acquire each of these digital surfaces because only points simultaneously visible in two cameras could be recorded in a single measurement. Error accumulation occurs in the cloud data registration, 3–5 measurements were needed to acquire a complete joint surface,

the combined three-dimensional error accumulation and its influence on roughness measurements are difficult to quantify, but as a worst case, the final accuracy can be decided as 0.1 mm, which is the same with Indraratna’s study, so the zones where $-0.1 \text{ mm} < z_{\text{deviation}} < 0.1 \text{ mm}$ are assumed to be uninfluenced zones.

2. The void space of a joint can be represented by the aperture distribution, which was calculated by aligning the upper and lower joint surface data after the test to the initial closed joint model and then moving the upper joint surface according to the normal and shear displacements throughout the experimental procedure (Fig. 2b). Thus, the joint aperture distribution (z_{aperture}) of the joint was presented by

$$z_{\text{aperture}}(x_i, y_i) = z_{\text{after_upper}}(x_i + dx, y_i) + dz - z_{\text{after_lower}}(x_i, y_i) \quad (2)$$

where $z_{\text{after_upper}}(x_i + dx, y_i)$ is the asperity height of the upper joint surface moved according to the shear displacement dx after being aligned to the closed joint model, $z_{\text{after_lower}}(x_i, y_i)$ is the asperity height of the lower joint surface after being aligned to the closed joint model, dz is the normal displacement of the upper joint surface caused by initial normal and shear loads, $dz > 0$ represents normal dilation, and $dz < 0$ represents normal compression.

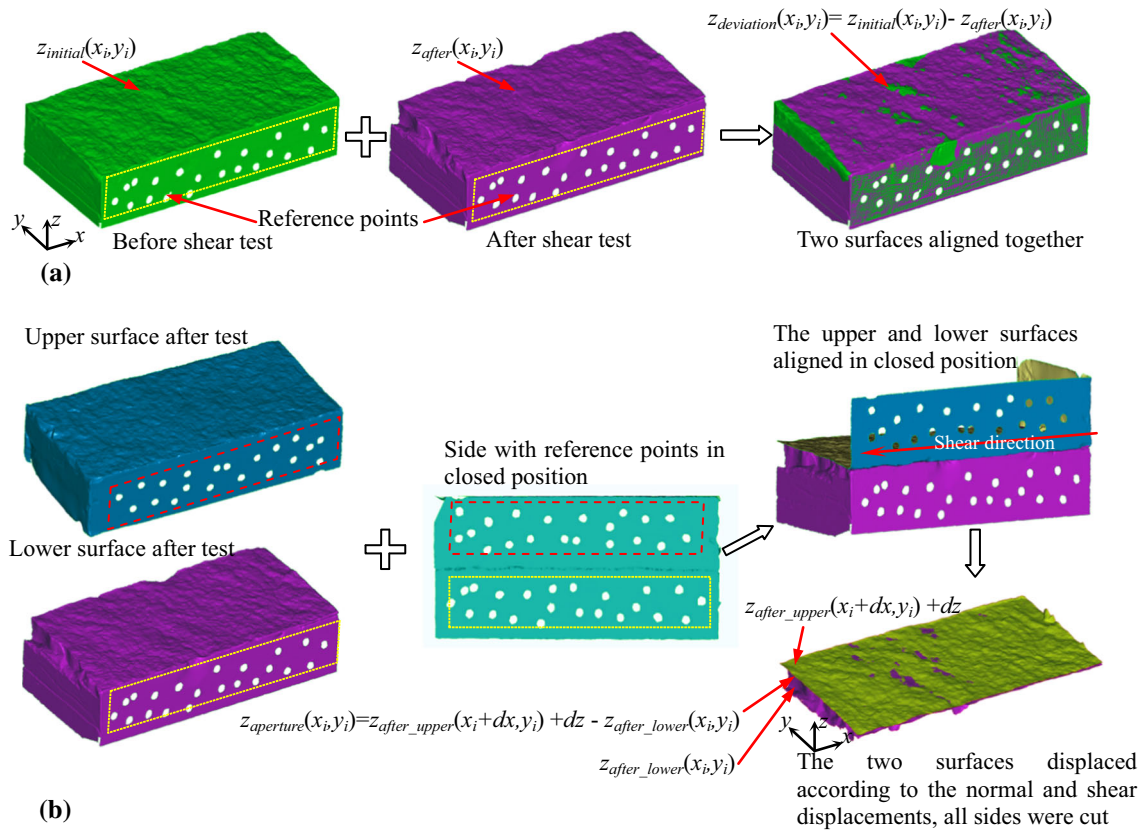


Fig. 2 **a** The alignment of the joint surfaces before and after shear test of the lower surfaces of WJ-1, **b** procedure for acquiring joint aperture distribution of WJ-1 during shearing

5 Results and Discussion

5.1 Verification of the Proposed Method

To control the independent parameters governing the rock joint shear behavior, plaster replicas of natural joint were used in this study, and the use of joint replicas had been frequently used in the previous study (Riss et al. 1997; Yang et al. 2010; Hossaini et al. 2014; Indraratna et al. 2014). Here, to prove the reproducibility of specimen preparing, 3D roughness parameter C and 2D roughness parameter JRC (joint roughness coefficient, Barton and Choubey 1977), were employed to characterize the replicated joint surface topography. Grasselli et al. (2002) proposed the concept of the joint surface apparent dip angle θ facing against the shear direction. Grasselli obtained the relationship between the potential contact area A_θ and the corresponding minimum apparent dip angle θ :

$$\frac{A_\theta}{A_0} = \left(\frac{\theta_{\max} - \theta}{\theta_{\max}} \right)^C \tag{3}$$

where A_θ is the potential contact area which is the sum area of surface elements with apparent dip angle larger than θ , A_0 is the maximum possible contact area along shear

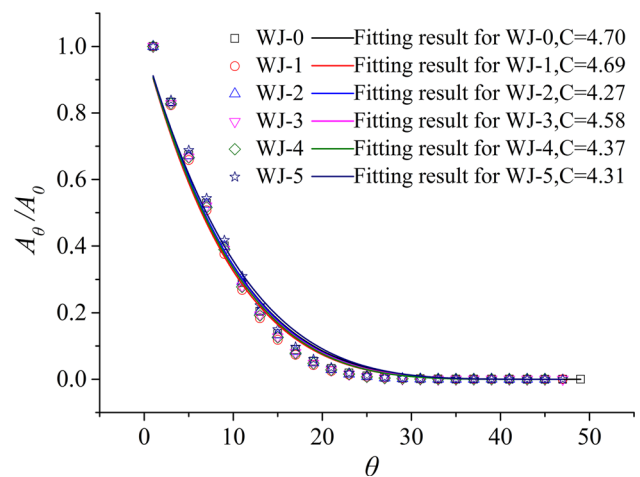


Fig. 3 Fitting results of A_θ/A_0 and θ by Eq. 3

direction, θ_{\max} is the maximum apparent dip angle, C is the roughness parameter calculate by regression. Figure 3 shows the apparent dip angle distribution and the corresponding regression result of each specimen. The 3D roughness parameter C obtained from regression lie in the narrow range of 4.27–4.70.

Table 2 Shear test results

Specimen	Loading condition		Calculated average JRC		Experimental results	
	Normal stress/ MPa	Shear displacement/ mm	JRC _{before shear}	JRC _{after shear}	Peak shear displacement/ mm	Peak shear stress/ MPa
WJ-0	1	10.00	5.96	5.08	0.73	1.47
WJ-1		10.00	5.93	5.06	0.70	1.41
WJ-2		5.00	5.90	5.1	1.09	1.51
WJ-3		2.00	5.77	5.13	0.89	1.40
WJ-4		0.95	5.72	5.66	0.90	1.54
WJ-5		0.40	5.73	5.63	/	/

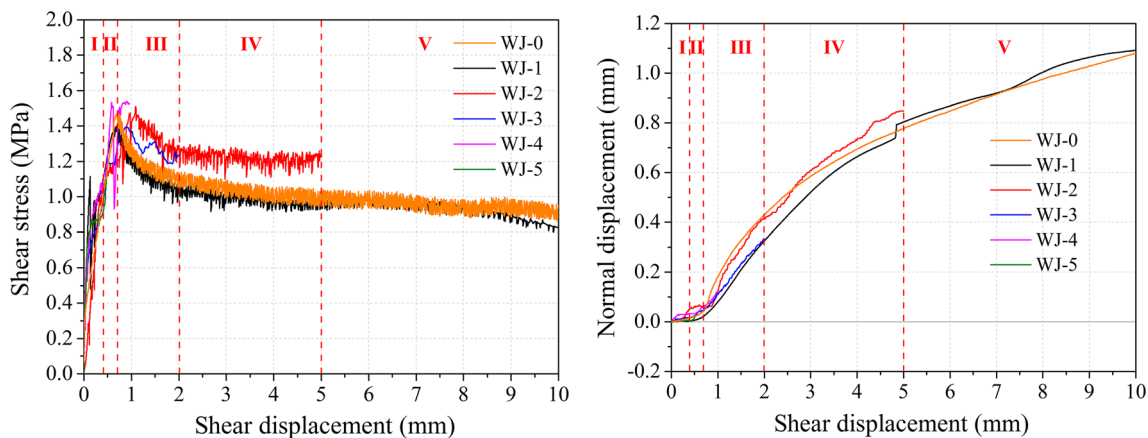


Fig. 4 Direct shear test results. The results were directly exported from the data acquisition system without embellishment

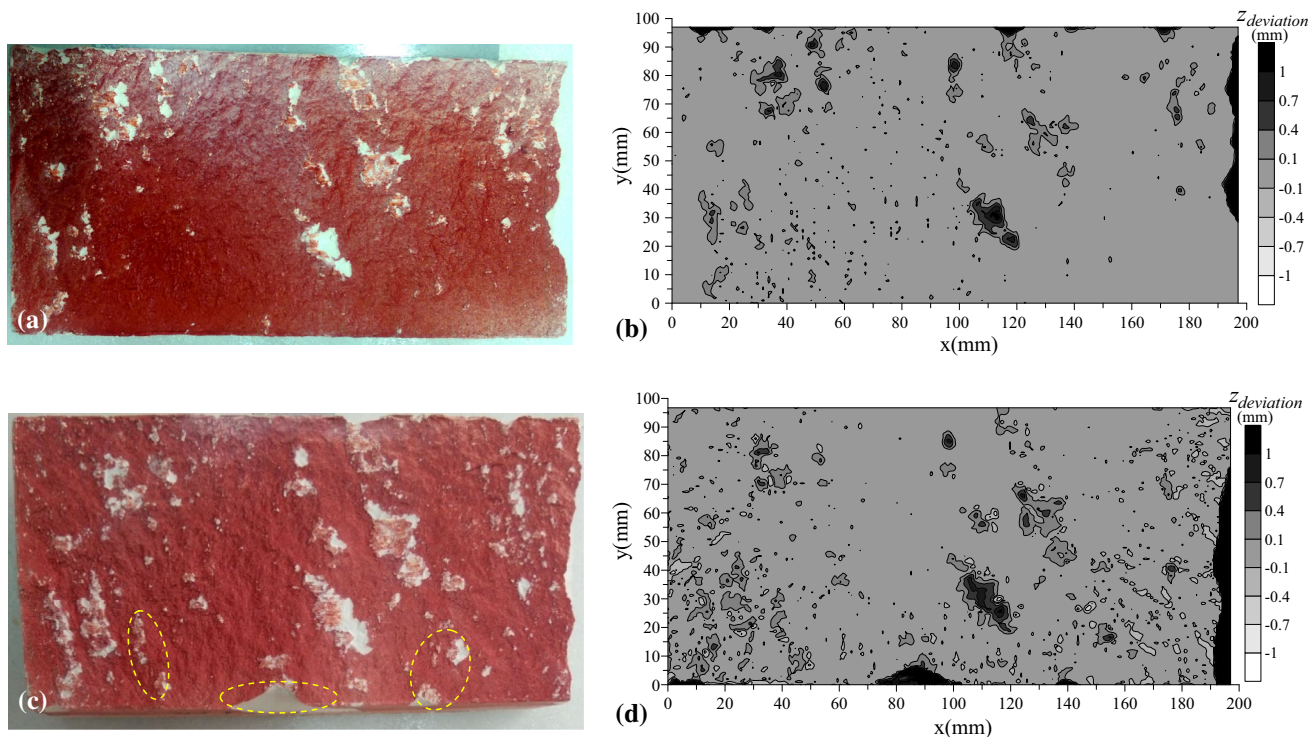



Fig. 5 Comparison of photograph after shearing and contour maps of asperity deformation calculated by the proposed method of the lower surface. **a** Photograph of WJ-0, **b** contour map of WJ-0, **c** photograph of WJ-1, **d** contour map of WJ-1

Shear direction of upper surface 

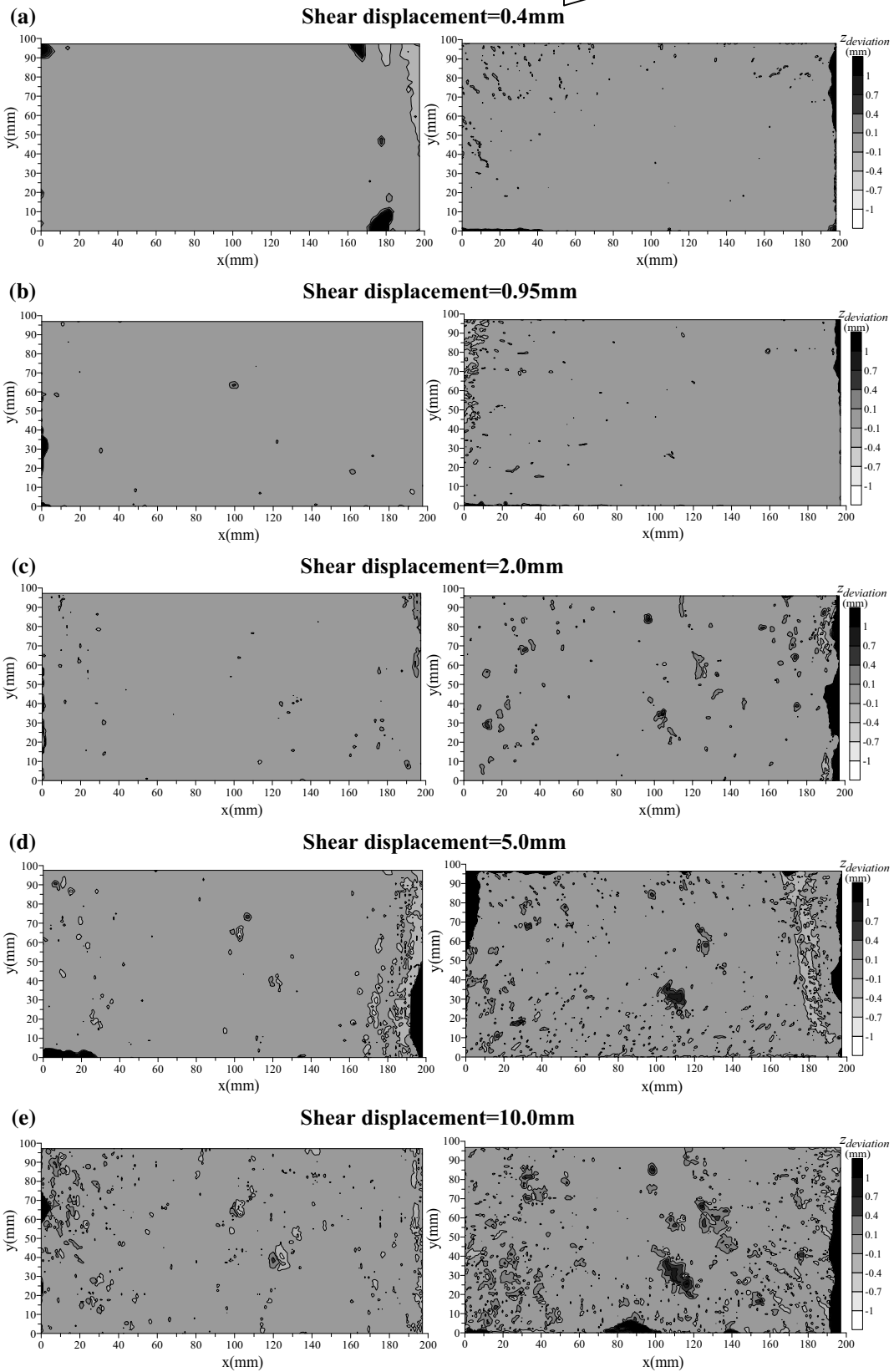


Fig. 6 Contour maps of surface asperity deformation. *Upper surfaces (left) and lower surfaces (right) under shear displacements of a 0.4 mm (WJ-5), b 0.95 mm (WJ-4), c 2.0 mm (WJ-3), d 5.0 mm (WJ-2), and e 10.0 mm (WJ-1)*

Tse and Cruden (1979) proposed an empirical statistical relationship between the JRC and Z_2 (the root-mean-square of the first derivative of the profile) to calculate typical JRC values:

$$JRC = 32.2 + 32.47 \log Z_2 \tag{4}$$

where Z_2 can be calculated in the following discrete form:

$$Z_2 = \left[\frac{1}{L} \sum_{i=1}^{N-1} \frac{(z_{i+1} - z_i)^2}{(x_{i+1} - x_i)} \right]^{0.5} \tag{5}$$

where (x_i, z_i) represent the coordinate of the points of the profile, N is the total number of points in the profile, and L is the length of the profile. The JRC was the length-weighted average value of all the roughness profiles spaced at 0.5 mm parallel to shear direction. Results of 2D joint surface roughness JRC before shearing are shown in Table 2; JRC of all the specimens lies in the narrow range of 5.72–5.96. The JRC and C calculation results prove the reproducibility of our method of specimen preparing.

Two tests, WJ-0 and WJ-1, were conducted under 1 MPa normal stress and stopped at 10.0 mm shear displacement to verify the repeatable of direct shear test and surface evolution calculation method. The two complete shear test results can be found in Fig. 4. Figure 5a, c show the photographs of the lower surfaces of the WJ-0 and WJ-1 after shearing, respectively. The white zones visually illustrate the areas where the surface of the joint has undergone deformation; Fig. 5b, d show the corresponding contour map of the asperity deformation distribution. The calculated deformed areas in Fig. 5b, d are consistent with

the observed deformed areas in Fig. 5a, c, respectively. Figure 5a, c is consistent except the zones represented by elliptical lines; this discrepancy was due to many factors (void spaces in specimen after molding, drying conditions, or any impurity in plaster material) would influence the test result, even though great lengths were taken to be as consistent as possible, but not all the variables could be completely controlled.

5.2 Joint Shear Behavior

The complete shear test until reaching the residual shear strength state was first conducted to determine the shear displacements the subsequent tests should be stopped at. The two complete shear tests results, WJ-0 and WJ-1, are shown in Fig. 4. According to the shear stress–shear displacement and the normal displacement–shear displacement relationships, the whole shear processes can be divided into the following five phases:

Phase I: The elastic mobilization phase with a linear shear stress–shear displacement relationship.

Phase II: The pre-peak shear stress phase characterized by shear stress increases nonlinearly with shear displacement, dilation started increase at the end of this phase.

Phase III: The rapid softening phase characterized by nonlinear shear stress that decreases under a decreasing shear stress gradient.

Phase IV: The linear softening phase with shear stress decreases toward residual shear stress under an almost constant shear stress gradient.

Phase V: This phase involves the residual strength phase of upper joint that stably slides on the lower joint.

The above analysis shows four shear displacements (or shear stresses) where the significant joint surface

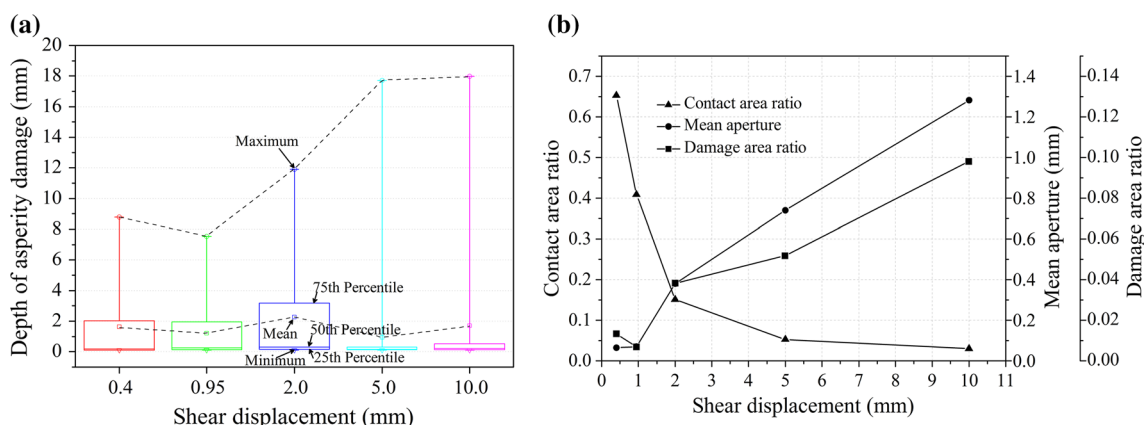


Fig. 7 **a** Box and whisker plots of depth of asperity damage for lower joint surfaces under different shear displacements, **b** change of contact area ratio, mean aperture and damage area ratio for lower joint surfaces at different shear displacements

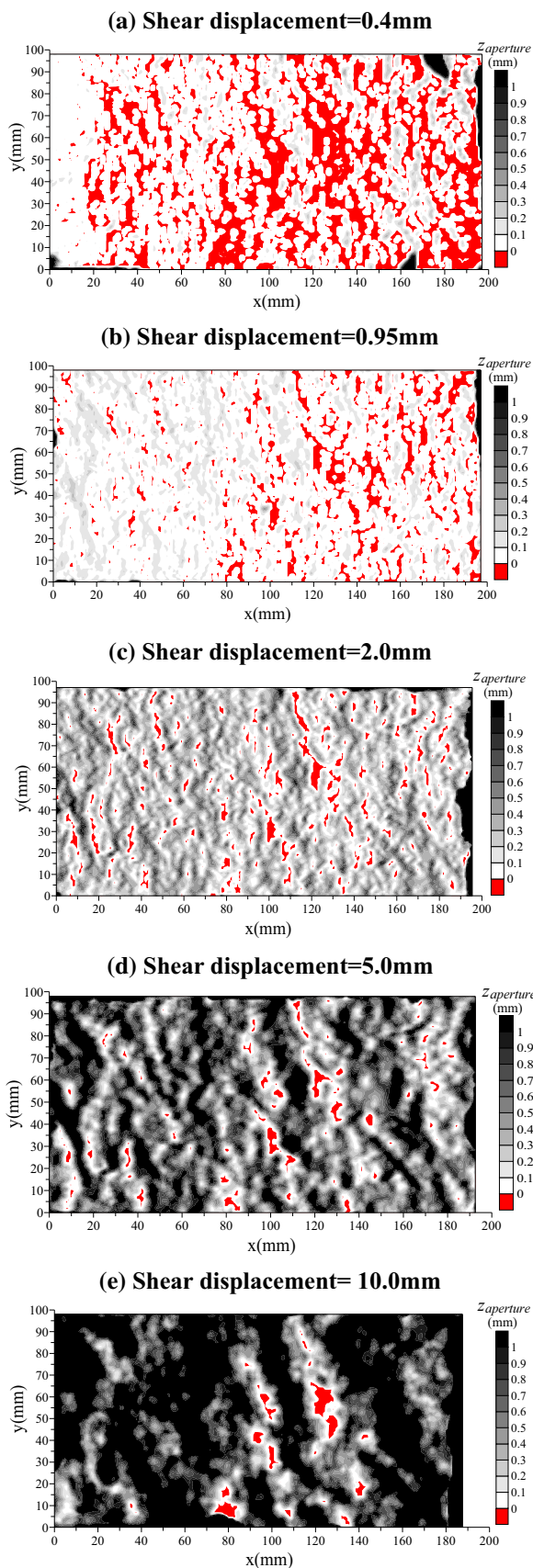


Fig. 8 Evolution of contour maps of aperture distribution under shear displacements of **a** 0.4 mm (WJ-5), **b** 0.95 mm (WJ-4), **c** 2.0 mm (WJ-3), **d** 5.0 mm (WJ-2), **e** 9.4 mm (WJ-1). Red color in the contour maps represents the contact area (color figure online)

deformations are most likely to occur. The analysis specified that the subsequent shear tests should be stopped at the following shear displacements to study the joint surface evolution during shearing: 0.4 mm shear displacement (WJ-5), peak shear displacement (WJ-4), 2.0 mm shear displacement (transition from decreasing shear stress gradient to a constant, WJ-3), and 5.0 mm shear displacement (shear stress came to residual strength phase, WJ-2).

The subsequent test results can also be found in Fig. 4 and Table 2. WJ-1–WJ-4 show similar shear stress–shear displacement relationship, but their peak shear stresses vary from 1.40 to 1.69 MPa; this variation resulted from unpredicted variables throughout shear tests that could not be completely controlled.

5.3 Joint Surface Degradation and Void Space Evolution

Figure 6 shows the contour maps of surface degradation with shearing. It is clear that the surface damage of the lower surface had relative clear degradation regularity than that of the upper surface. Thus, the lower surface was more suitable for further study of the joint surface degradation. Note that after shear test and before surface scanning, joint surfaces were cleaned by a soft brush to sweep the debris that were just on the surfaces and they were not compacted and attached to the joint surfaces. Some slightly attached debris may have been swept in this procedure, causing irregularity of the deformation of the upper surfaces, which were dominated by debris accumulation. Figure 7a shows the box and whisker diagrams illustrating the depth of asperity damage on the lower surfaces. The mean asperity damage depth was close to 0.1 mm at 0.4 mm shear displacement, which indicates that most asperities of the joint surface were in their integrity and undistorted. The mean asperity damage depth reached 2.3 mm at 2.0 mm displacement. Then, the mean asperity damage depth decreased and tended to be constant of approximately 1.0–1.8 mm. However, the maximum asperity damage depth increased before reaching 5.0 mm shear displacement and then remained constant afterward; thus, the maximum asperity depth peaked after the mean asperity damage depth did. This condition was attributed to that even though the maximum asperity damage height increased until 5.0 mm shear displacement, the new weak damage area increased rapidly, which offset and even exceeded the further asperity damage on existing damage

zones. The rapid increase in the new damage area can be seen in Fig. 7b.

Figure 8 shows the void space at different shear displacements. Figure 8 shows that the contact area and the joint aperture aligned perpendicularly to the shear direction and interlaced with one another. The contact areas decreased all the way from evenly distributed in the joint surface until the 10.0 mm shear displacement of a few large isolated patches but were still perpendicularly aligned to the shear direction. The decreasing of the joint contact area ratios can be seen in Fig. 7b, where the joint contact area ratios dropped sharply before 2.0 mm shear displacement, then decreased slowly with a decreasing gradient approaching 0.

6 Conclusions

A new method for estimating the joint surface and void space evolution was presented in detail in this study. Surface roughness calculation and repeat tests were conducted to prove the reproducibility of the new method. Several preliminary applications of the method were also introduced, and the results were analyzed. From the test result, the new method was able to capture the damage area and damage degree of the joint surface during shearing. Although this study places an emphasis on the joint surface damage under shear, the proposed method is more promising in investigating the evolution of the joint shear mechanical related surface roughness parameters, studying the relationship between the changing parameters and the joint shear behavior, and ultimately deriving the constitutive model for shear stress–shear displacement. More importantly, the determination of the joint surface geometry and joint aperture distribution during shearing provides a basic requirement for joint shear-flow research and related numerical simulations.

Acknowledgements This study was supported by the National Natural Science Foundation of China (No.41327001, No.41472248).

References

Archambault G, Gentier S, Riss J, Flamand R (1997) The evolution of void spaces (permeability) in relation with rock joint shear behavior. *Int J Rock Mech Min Sci* 34(3–4):14.e1–14.e15

Asadollahi P, Tonon F (2010) Constitutive model for rock fractures: revisiting Barton's empirical model. *Eng Geol* 113(1):11–32

Bandis SC, Lumsden AC, Barton N (1983) Fundamentals of rock joint deformation. *Int J Rock Mech Min Sci Geomech Abstr* 20(6):249–268

Barton N, Choubey V (1977) The shear strength of rock joints in theory and practice. *Rock Mech Rock Eng* 10(1):1–54

Belem T, Mountaka S, Homand EF (2007) Modeling surface roughness degradation of rock joint wall during monotonic and cyclic shearing. *Acta Geotech* 2(4):227–248

Belem T, Souley M, Homand EF (2009) Method for quantification of wear of sheared joint walls based on surface morphology. *Rock Mech Rock Eng* 42(6):883–910

Fathi A, Moradian Z, Rivard P, Ballivy G, Boyd AJ (2015) Geometric effect of asperities on shear mechanism of rock joints. *Rock Mech Rock Eng* 49:1–20

Gentier S, Billaux D, Vliet LV (1989) Laboratory testing of the voids of a fracture. *Rock Mech Rock Eng* 22(2):149–157

Goodman RE (1989) *Introduction to rock mechanics*, 2nd edn. Wiley, New York

Grasselli G, Egger P (2003) Constitutive law for the shear strength of rock joints based on three-dimensional surface parameters. *Int J Rock Mech Min Sci* 40(1):25–40

Grasselli G, Wirth J, Egger P (2002) Quantitative three-dimensional description of a rough surface and parameter evolution with shearing. *Int J Rock Mech Min Sci* 39(6):789–800

Hans J, Boulon M (2003) A new device for investigating the hydro-mechanical properties of rock joints. *Int J Numer Anal Meth Geomech* 27(27):513–548

Hossaini KA, Babanouri N, Nasab SK (2014) The influence of asperity deformability on the mechanical behavior of rock joints. *Int J Rock Mech Min Sci* 70(9):154–161

Indraratna B, Thirukumar S, Brown ET, Premadasa W, Gale W (2014) A technique for three-dimensional characterization of asperity deformation on the surface of sheared rock joints. *Int J Rock Mech Min Sci* 70(9):483–495

Koyama T, Fardin N, Jing L, Stephansson O (2006) Numerical simulation of shear-induced flow anisotropy and scale-dependent aperture and transmissivity evolution of rock fracture replicas. *Int J Rock Mech Min Sci* 43(1):89–106

Kulatilake PHSW, Balasingam P, Park J, Morgan R (2006) Natural rock joint roughness quantification through fractal techniques. *Geotech Geol Eng* 24(5):1181–1202

Kulatilake PHSW, Park J, Balasingam P, Morgan R (2008) Quantification of aperture and relations between aperture, normal stress and fluid flow for natural single rock fractures. *Geotech Geol Eng* 26(3):269–281

Ladanyi B, Archambault G (1970) Simulation of shear behavior of a jointed rock mass. In: *Proceedings of the 11th US Symp on Rock Mechanics*, pp 105–125

Li B, Jiang J, Koyama T, Jing R, Tanabashi Y (2008) Experimental study of the hydro-mechanical behavior of rock joints using a parallel-plate model containing contact areas and artificial fractures. *Int J Rock Mech Min Sci* 45(3):362–375

Nemoto K, Watanabe N, Hirano N, Tsuchiya N (2009) Direct measurement of contact area and stress dependence of anisotropic flow through rock fracture with heterogeneous aperture distribution. *Earth Planet Sci Lett* 281(1–2):81–87

Olsson R, Barton N (2001) An improved model for hydromechanical coupling during shearing of rock joints. *Int J Rock Mech Min Sci Geomech Abstr* 38(3):317–329

Park JW, Song JJ (2013) Numerical method for the determination of contact areas of a rock joint under normal and shear loads. *Int J Rock Mech Min Sci* 58(7):8–22

Park JW, Lee YK, Song JJ, Choi BH (2013) A constitutive model for shear behavior of rock joints based on three-dimensional quantification of joint roughness. *Rock Mech Rock Eng* 46(6):1513–1537

Riss J, Gentier S, Archambault G (1997) Sheared rock joints: dependence of damage zones on morphology anisotropy. *Int J Rock Mech Min Sci* 34(3–4):258

Tse R, Cruden DM (1979) Estimating joint roughness coefficients. *Int J Rock Mech Min Sci Geomech Abstr* 16:303–307

- Xia CC, Tang ZC, Xiao WM, Song YL (2014a) New peak shear strength criterion of rock joints based on quantified surface description. *Rock Mech Rock Eng* 47(2):387–400
- Xia CC, Gui Y, Wang W, Du SG (2014b) Numerical method for estimating void spaces of rock joints and the evolution of void spaces under different contact states. *J Geophys Eng* 11(11):065004
- Yang ZY, Taghichian A, Li WC (2010) Effect of asperity order on the shear response of three-dimensional joints by focusing on damage area. *Int J Rock Mech Min Sci* 47(6):1012–1026
- Zandarin MT, Alonso E, Olivella S (2013) A constitutive law for rock joints considering the effects of suction and roughness on strength parameters. *Int J Rock Mech Min Sci* 60(2):333–344